JUSTC

Article

http://justc.ustc.edu.cn

In situ electrochemical detection of the interface between single-layer graphene/[EMI$^+$][TFSI$^-$] ionic liquids

Na Shu[1], Baiquan Zhu[2], Xiaolan Wang[1], Yanxia Chen[2], Kun Ni[1] ✉, Simon Patrice[3], and Yanwu Zhu[1,4] ✉

[1]*Department of Materials Science and Engineering, School of Chemistry and Materials Science, University of Science and Technology of China, Hefei 230026, China;*
[2]*Hefei National Research Center for Physical Sciences at the Microscale, University of Science and Technology of China, Hefei 230026, China;*
[3]*CIRIMAT UMR CNRS 5085, Université Paul Sabatier, 118 route de Narbonne, 31062 Toulouse, France; Réseau sur le Stockage Electrochimique de l'Energie (RS2E), CNRS FR3459, 80039 Amiens, France;*
[4]*Key Laboratory of Precision and Intelligent Chemistry, University of Science and Technology of China, Hefei, Hefei 230026, China*

✉Correspondence: Kun Ni, E-mail: nikun@ustc.edu.cn; Yanwu Zhu, E-mail: zhuyanwu@ustc.edu.cn

Graphical abstract

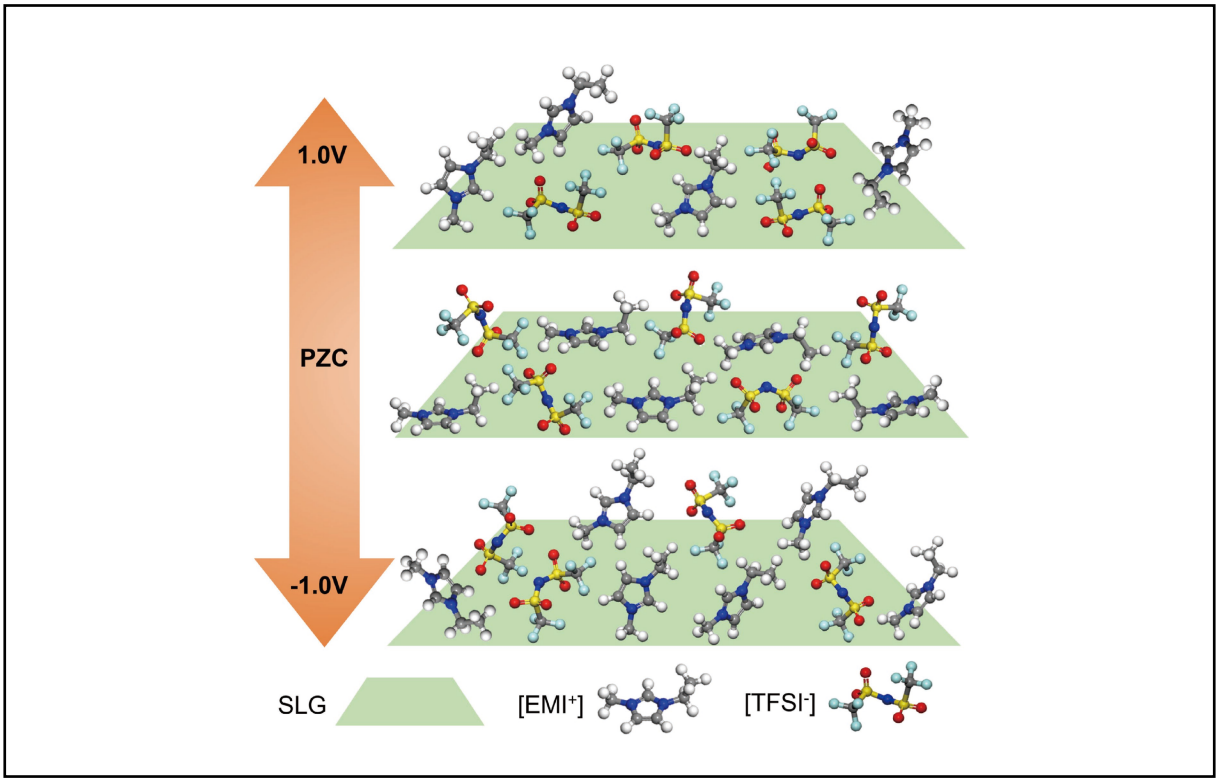

A potential-dependent reorientation of ions on the SLG/[EMI$^+$][TFSI$^-$] interface.

Public summary

- SLG has irreversible electrochemical doping during charge/discharge within −1–1 V and an irreversible structural change in the voltage range of >1.75 V or <−2.0 V.
- The imidazolium ring of [EMI$^+$] is tilted at low negative and positive polarization and then lifts away from the SLG surface at a higher positive potential (>0.6 V).
- The rearrangement of [TFSI$^-$] causes an increased adsorption density at positive potentials.

Citation: Shu N, Zhu B Q, Wang X L, et al. In situ electrochemical detection of the interface between single-layer graphene/[EMI$^+$][TFSI$^-$] ionic liquids. *JUSTC*, **2026**, 55(0): . CSTR: 32290.14.JUSTC-2024-0135. DOI: 32290.14.JUSTC-2024-0135

JUSTC

Article

http://justc.ustc.edu.cn

In situ electrochemical detection of the interface between single-layer graphene/[EMI$^+$][TFSI$^-$] ionic liquids

Na Shu[1], Baiquan Zhu[2], Xiaolan Wang[1], Yanxia Chen[2], Kun Ni[1] ✉, Simon Patrice[3], and Yanwu Zhu[1,4] ✉

[1]*Department of Materials Science and Engineering, School of Chemistry and Materials Science, University of Science and Technology of China, Hefei 230026, China;*
[2]*Hefei National Research Center for Physical Sciences at the Microscale, University of Science and Technology of China, Hefei 230026, China;*
[3]*CIRIMAT UMR CNRS 5085, Université Paul Sabatier, 118 route de Narbonne, 31062 Toulouse, France; Réseau sur le Stockage Electrochimique de l'Energie (RS2E), CNRS FR3459, 80039 Amiens, France;*
[4]*Key Laboratory of Precision and Intelligent Chemistry, University of Science and Technology of China, Hefei, Hefei 230026, China*

✉Correspondence: Kun Ni, E-mail: nikun@ustc.edu.cn; Yanwu Zhu, E-mail: zhuyanwu@ustc.edu.cn

Cite This: *JUSTC*, **2026**, 55(X): (8pp) Read Online SI Supporting Information

Abstract: A molecular-level understanding of the electrical double layer (EDL) on graphene is critical for the electrochemical energy storage of carbon-based electrodes. In this work, the electrochemical interface between single-layer graphene (SLG) and an ionic liquid (IL, [EMI$^+$][TFSI$^-$]) electrolyte is investigated by using cyclic voltammetry, electrochemical impedance spectroscopy, in situ Raman spectroscopy and in situ attenuated total internal reflection Fourier transform infrared (ATR-FTIR) spectroscopy. In the charge/discharge voltage range of −1.0 to 1.0 V, the SLG is electrochemically doped due to the interaction between adsorbed ions and SLG. For a voltage larger than 1.75 V or lower than −2.0 V, the irreversible formation of structural defects is detected on SLG, attributed to the decomposition of [EMI$^+$][TFSI$^-$] and the sequential reaction. In situ ATR-FTIR suggests a potential-dependent reorientation of ions: the imidazolium ring of [EMI$^+$] is tilted at low negative and positive polarization and then lifts away from the SLG surface at a higher positive potential (> 0.6 V), and the rearrangement of [TFSI$^-$] causes an increased adsorption density at positive potentials. Our findings provide deeper insight into the EDL structure on graphene down to the molecular level and may impact the design of carbon supercapacitors with higher energy storage capacity.

Keywords: graphene; ionic liquid; interface; electrochemistry

CLC number: **Document code:** A

1 Introduction

Electrochemical double-layer capacitors (EDLCs) store energy via an electrical double layer (EDL) formed by the adsorption of electrolyte ions on the surface of conductive electrodes and can charge or discharge within seconds. On a graphene electrode, a theoretical capacity of ~550 F·g^{-1} (21 μF·cm^{-2}) has been proposed, based on a specific surface area of ~2630 m^2·g^{-1} and a voltage of −0.6 V–0 V in 1-butyl-3-methylimidazolium hexafluorophosphate ([BMIM$^+$][PF$_6^-$]) ionic liquid (IL), which makes carbon-based EDLCs potentially competitive to lead acid batteries yet with a much higher power capacity[1]. In addition to the high electrical conductivity and excellent chemical stability, the specific surface area of carbon-based materials can be tailored to values above 3000 m^2·g^{-1}, such as in the situations of template-based porous carbon[2], biomass-derived porous carbon[3], mesoporous carbon nanofiber[4] and activated microwave exfoliated graphene oxide[5], bringing a wide interest of research on carbon-based electrodes. However, even leaving questions such as electrode loading alone[6], previously reported performances of carbon-based EDLCs are still far from expectations[1,7–9].

Considering the possible mechanisms behind this situation, the electrochemical performance of EDLCs is closely related to the electrochemical interface between the electrode and electrolyte, dominated by the EDL capacitance mainly from the adsorbed ions[10,11] and the quantum capacitance related to the carrier density change of the electrode[12,13]. Due to the complicated interaction between the charged ions in the EDL or between ions and electrode, understanding the electrochemistry of the carbon/electrolyte interface at the microscale remains a big challenge[6,14]. Numerous empirical observations have shown that the mechanisms of charge storage in nanoconfined space involve the comparison of pore/ion sizes[15,16], exchange processes of co/counter ions[17,18], desolvation effects[19,20], and so on. For example, Tsai et al.[18] investigated the adsorption/desorption behavior of [EMI$^+$][TFSI$^-$] (1-ethyl-3-methylimidazolium bis(trifluoromethylsulfonyl)imide) in carbide-derived carbon with pore sizes of 1 nm and 0.65 nm by electrochemical quartz crystal microbalance (EQCM), showing that ions cannot enter the pores when the size of ions is larger than the pore size. Further analysis indicates that only [EMI$^+$] is adsorbed on the negative electrode, and an exchange of [EMI$^+$] and [TFSI$^-$] occurs for small positive charges (ΔQ < 0.4 mC), while [TFSI$^-$] adsorption is

CSTR: 32290.14.JUSTC-2024-0135
DOI: 32290.14.JUSTC-2024-0135
JUSTC, **2026**, 55(X):

dominant for higher positive polarization. By combining in situ small-angle X-ray scattering and Monte Carlo simulations, Prehal et al.[19] showed that the desolvation of Cs^+ and Cl^- ions in H_2O is more significant when the average pore size of porous carbons decreases, and a partial desolvation of ions occurs in activated carbons even for a pore size larger than 1 nm.

At the molecular scale, charge screening[21,22] and ionic rearrangement[23–25] may have a significant influence on capacitance and ion dynamics. For example, using in situ X-ray reflectivity and molecular dynamics (MD) simulation, Uysal et al.[23] showed that the EDL features an alternating anion/cation layer structure at the epitaxial few-layer graphene/[C_9mim^+][Tf_2N^-] (1-methyl-3-nonylimidazolium bis(trifluoromethanesulfonyl)imide) interface. The slow time component (>10 s) in the dynamical response to potential and the hysteresis in cyclic voltammetry (CV) scans at 100 mV·s^{-1} have been attributed to the structural reorganization of EDL, where the imidazolium rings of [C_9mim^+] and the alkyl tails prefer to lie parallel to the graphene surface at −0.4 V and [Tf_2N^-] has two different orientations at 1.0 V. Zhou et al.[25] characterized the EDL of [EMI^+][$TFSI^-$] on highly ordered pyrolytic graphite (HOPG) by atomic force microscopy, suggesting that the EDL consists of multiple discrete ionic layers, where the potential-dependent structural reconfiguration occurs in the first layer of EDL; MD simulation revealed that [EMI^+] is parallel to the HOPG and [$TFSI^-$] is vertical at a charge density of −0.55 e·nm^{-2}, while [EMI+] becomes vertical and [$TFSI^-$] becomes flatter on the HOPG surface at 0.55 e·nm^{-2}.

Compared to carbons with a confined space and complicated EDL[10,26], high-quality single-layer graphene (SLG) can largely exclude the influence of curvature, pores, defects and dopants, enabling better monitoring of ion desolvation, exchange and rearrangement and potentially allowing for a more intrinsic understanding of charge storage mechanisms on carbon surfaces. Among several theoretical studies, Paek et al.[27] demonstrated the distinct alternative layering of [$BMIM^+$] and [PF_6^-] (1-butyl-3-methyl-imidazolium hexafluorophosphate, $BMIMPF_6$) near a polarized graphene surface, where [$BMIM^+$] tends to align parallel to the graphene when the charged density (σ) is −10 μC·cm^{-2}, the alkyl tails bend away from the surface and the rings become tilted when σ = −40 μC·cm^{-2}. Previous reports indicated that the EDL structure at the graphene/IL interface probed by sum frequency generation spectroscopy (SFG) or X-ray reflectivity (XR) has alternating anion/cation layers and restructuring by external potential variation[28–30]. In particular, Xu et al.[30] indicated that the anion concentration and the orientation distribution on the surface probed by SFG change with the applied potential, while the cation methyl and methylene surface concentrations do not show significant sensitivity on the triple layer graphene/[BMIM][DCA] (1-butyl-3-methylimidazolium dicyanamide) interface. With EQCM, Ye et al.[31] proposed a cluster-like desorption of [$EMI_{1.58}$,$TFSI_{0.58}$]$^+$ for positive polarization and an ionic reorganization for negative polarization, i.e., a relocation of ions without changing the mass of adsorbed ions, on SLG made by chemical vapor deposition (CVD). In addition, Wu et al.[32] highlighted the screening effect of acetonitrile, which thus significantly alters the interaction between [EMI^+][$TFSI^-$] and SLG. Although the proceedings above, the spatial arrangement and tilting of ions on graphene down to the molecular level has rarely been observed, requiring a more subtle characterization technique to detect the electrochemical interface on graphene.

In this work, we utilize in situ attenuated total internal reflection Fourier transform infrared (ATR-FTIR) spectroscopy combined with electrochemical measurements and in situ Raman spectroscopy to investigate the potential-dependent ionic behavior of [EMI^+][$TFSI^-$] on SLG made by CVD. We find that SLG is first doped due to the interfacial interaction between the IL and graphene under potentials of −1.0 V to 1.0 V. Then, the SLG experiences an irreversible structural change when the voltage range increases to above 1.75 V or below −2.0 V due to the decomposition of [EMI^+][$TFSI^-$] and the reaction with carbon. ATR-FTIR spectroscopy reveals a potential-dependent orientation of ions, where the imidazolium ring of [EMI^+] becomes tilted under negative or positive polarization, while the rearrangement of [$TFSI^-$] causes increased adsorption density under positive polarization on the SLG surface.

2 Experimental section

2.1 Transfer of SLG

The SLG films were obtained by chemical vapor deposition (CVD) on a copper (Cu) substrate (Roucarbon Technology, Ningbo). After spin-coating PMMA (30 mg·mL^{-1}) on one side of SLG on Cu, the copper was etched by 0.5 M ammonium persulfate ($(NH_4)_2S_2O_8$). The PMMA-coated SLG was rinsed with DI water and transferred to a SiO_2 substrate with patterned Cr/Au (thickness: 5/50 nm, width: 10 μm) leads, which were deposited by ultraviolet lithography. The as-transferred PMMA/SLG was dried in ambient conditions and then baked at 180 °C for 2 h. Finally, the PMMA was removed by acetone (4 h soaking) and isopropanol (30 min soaking) at room temperature and then blow-dried under nitrogen. The transfer process of SLG on the Au/SiO_2 substrate is shown in Fig. S1a (see Supporting information).

2.2 Electrochemical measurements

Cyclic voltammetry (CV) measurements were performed by using a three-electrode electrochemical cell, as shown in Fig. S1b, where the working electrode was SLG/Au/SiO_2, the counter and quasireference electrodes were both platinum wire, and the electrolyte was 1-ethyl-3-methylimidazolium bis(trifluoromethylsulfonyl)imide ([EMI^+][$TFSI^-$]). All CV measurements were in the scan rate range of ±1 V at 20 mV s^{-1}. Electrochemical impedance spectroscopy (EIS) measurements in [EMI^+][$TFSI^-$] were performed by using an ATR-FTIR electrochemical cell, as shown in Fig. 3a, where the working electrode was SLG/ZnSe. The frequency range of EIS was 1 Hz to 100 kHz, and the sinusoidal potential perturbation had an amplitude of 10 mV.

2.3 In situ Raman spectroscopy and ATR-FTIR

In situ electrochemical Raman spectroscopy was performed by an electrochemical cell, as shown in Fig. S2. The electrolyte was sealed by a layer of sealant and cover glass, and the

CSTR: 32290.14.JUSTC-2024-0135
DOI: 32290.14.JUSTC-2024-0135
JUSTC, **2026**, 55(X):

thickness of the electrolyte was ~100 μm. The Raman laser (532 nm) was focused on SLG through the SiO_2 crystal window. A potentiostat (Princeton Parstat 4000) was used to control the potential. After holding the constant potential for 60 s, Raman spectra were recorded at an acquisition time of 2 s and accumulations of 3 times using a 50x telephoto lens and 50% excitation power. In situ ATR-FTIR spectroscopic measurements were performed by using the ATR-FTIR device, as shown in Fig. 3a. IR spectra were recorded simultaneously in a potential sweep from 0 to +1.0/−1.0 V at a scan rate of 20 $mV \cdot s^{-1}$. All spectra were obtained by integrating 8 interferograms (ca. 3 s/per spetrum) at a resolution of 4 cm^{-1}. The background spectrum (R_0) was recorded at ~0 V, and the spectrum accumulated for 128 scans. All spectra were presented in absorbance, $A=\log(R_0/R)$, where R is the spectrum at applied potential. The experimental Raman and IR conditions did not cause significant damage to SLG, as shown by the Raman spectra in Fig. S3.

2.4 Simulation method

Density functional theory (DFT) simulations were performed by using the Vienna ab initio simulation package (VASP) software. The exchange-correlation interactions were described by generalized gradient approximation (GGA) with the Perdew-Burke-Ernzerhof (PBE) functional. The energy cutoff of the plane wave basis set was 500 eV. Gaussian-type smearing with an energy window of 0.05 eV was used. The energy convergence tolerance was 0.01 meV. The force tolerance for geometry optimization was 0.01 $eV \cdot Å^{-1}$. All calculations were performed with spin unrestricted. K points were sampled as gamma only. The dipole moment in *the x*, *y*, *z* direction is calculated by IDIPOL parameters in 1, 2, and 3, accompanied by DIPOL = 0.5 0.5 0.5 and LDIPOL = T.

The calculation of the refractive index of SLG was performed with VASP software. The primitive cell of graphene is used for the calculation. The energy cutoff of the plane wave basis set was 400 eV. A total of 80 bands (occupied and unoccupied together) were considered. The energy convergence tolerance was 10^{-8} eV. The charge injection was considered by adding additional electrons/holes into the system by the NELECT parameter. An automatic Gamma-centered K point mesh of 78×78×1 was used.

The orientation of the electron dipole moment for a certain vibration model is evaluated by the change in the dipole moment vector when vibration occurs. Assuming that the dipole moment vector in a fully relaxed molecule is n1, the dipole moment vector changes into n_2 when the vibration dynamical matrix for coordination (dx, dy, dz) is added into the model (x, y, z). Then, the electron dipole moment for a certain vibration model is defined by vector subtraction $n = n_2 - n_1$.

3 Results and discussion

The preparation of SLG is described in the Supporting Information. Ex situ Raman spectroscopy was first carried out on the SLG on quartz to verify the quality of SLG. The Raman spectrum shown in Fig. 1a reveals a typical feature of SLG with a G band at ~1588 cm^{-1} and a 2D band at ~2678 cm^{-1}. The high 2D/G intensity ratio (~2.76) and negligible D band suggest that the transferred SLG has a high quality and a very low defect level[33]. With $[EMI^+][TFSI^-]$ as the electrolyte, the cyclic voltammetry (CV) measurement of SLG (Fig. 1b) taken in a three-electrode electrochemical cell shows a typical EDL charging/discharging behavior, which is dominant in a potential range of ±1.0 V. The C–V curve has a slight fluctuation at ~ 0.7 V, which may be caused by the reconstructed structure and oxidation of the Au surface[34]. An obvious polarization is shown near ±1.0 V, while the structure of graphene is not significantly changed, as discussed below. The specific capacitance calculated from the CV curve is ~12 μF cm^{-2}, in agreement with our previously reported value obtained from the graphene/Au electrode[31].

In situ Raman spectroscopy was performed to show the structural evolution of SLG during electrical polarization at various potentials. SLG transferred to a quartz substrate was patterned with a Cr/Au (Au on Cr) bar (thickness: 5(Cr)/50(Au) nm, line width: 10 μm; Fig. S1a) and used as the working electrode, with platinum wires (diameter: 0.5 mm) as the counter and quasireference electrodes, as shown in Fig. S2. The electrochemical cell is shown in Fig. S1b. Fig. 2a shows that the position and intensity of the G and 2D peaks of SLG are sensitive to the potential, as guided by the dotted curves. From the summary of position changes in Fig. 2b, we can see that the shifts of the G and 2D peaks both have minimum values at approximately −0.3 V. The G and 2D peaks shift to higher wavenumbers by ~27 cm^{-1} and ~9 cm^{-1},

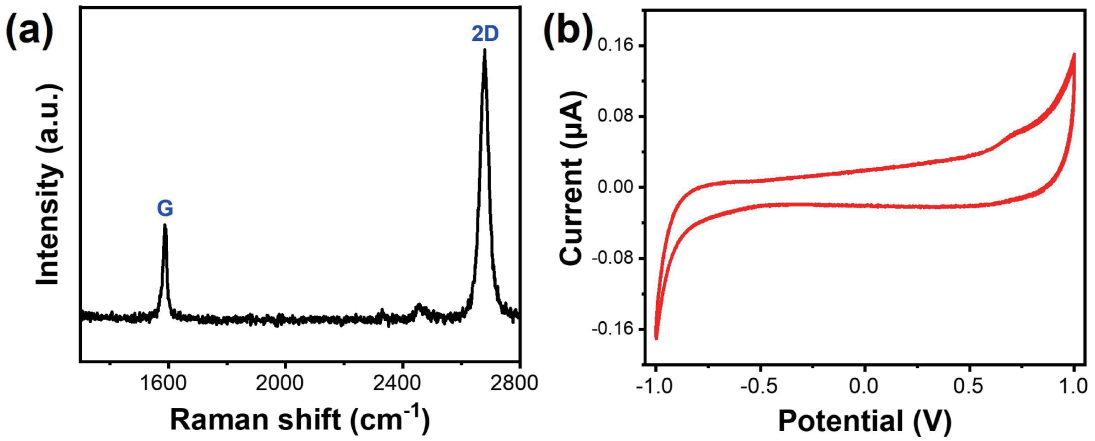

Fig. 1. (a) Typical Raman spectrum of SLG. (b) Cyclic voltammogram of SLG in $[EMI^+][TFSI^-]$ at a scan rate of 20 $mV \cdot s^{-1}$.

CSTR: 32290.14.JUSTC-2024-0135
DOI: 32290.14.JUSTC-2024-0135
JUSTC, **2026**, 55(X):

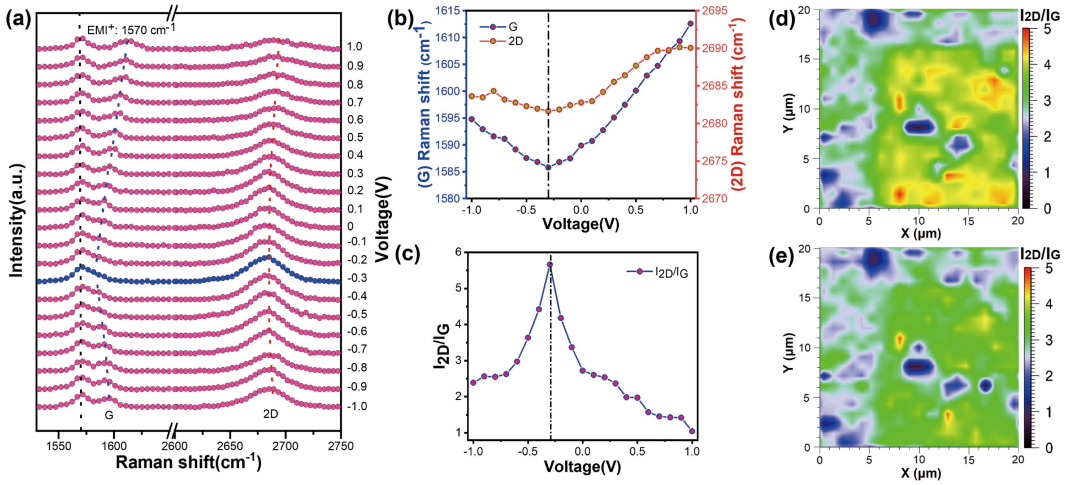

Fig. 2. (a) In situ Raman spectra of SLG in [EMI+][TFSI−] recorded at different potentials; the blue stippled curve corresponds to the Dirac point. (b) Positions of G and 2D bands and (c) intensity ratio of 2D to G (I_{2D}/I_G) as a function of potential. Raman mapping of I_{2D}/I_G in the same region (d) before and (e) after the electrochemical cycles.

respectively, under positive polarization due to hole doping[35–37]. Under negative polarization, the G peak shifts to ~1594 cm^{-1} due to electron doping, while the frequency of the 2D peak increases by ~3 cm^{-1} for the same reason[36,37]. In addition, electrochemical doping increases the number of carriers and thus the probability of scattering (the photogenerated electron-hole pairs scatter with doping-induced electrons or holes)[37,38], so the intensity ratio (I_{2D}/I_G) has a maximum at the Dirac point and decreases under polarization, as shown in Fig. 2c. The I_{2D}/I_G ratio has an inverse trend but a similar shape of capacitance curve relative to the potential, as shown in Fig. S4, indicating that C_Q, which is related to the interplay between the charge carriers in the SLG and the ions near SLG, has a dominant effect on the interfacial capacitance[36].

After the SLG experienced by 5 cycles of CV testing was washed with ethanol and blow-dried with nitrogen, ex situ Raman spectroscopy was performed in exactly the same region to further investigate the structural change of SLG, as shown in Fig. 2d and e. From the comparison, we can see that the I_{2D}/I_G ratio decreases after five electrochemical cycles, while the I_D/I_G ratio shows no significant change (Fig. S5), indicating that SLG has irreversible electrochemical doping but still maintains its structural integrity. The doping may be related to the adsorption of cations on SLG, involving the weak van der Waals interaction between the ionic liquid and graphene, as previously reported[39,40]. However, when the voltage increases to values higher than +1.75 V (or decreases to values lower than −2.0 V), the SLG experiences irreversible structural changes and generates a large number of defects, as indicated by the increase in I_D/I_G to ~1.0 (Fig. S6), which can be explained by the breaking of S=O bonds in [TFSI−] or the reaction between lost oxygen atoms and carbon atoms in graphene (or the reduction of [EMI+] to form a double-bond dimer)[41,42].

Electrochemical impedance spectroscopy (EIS) was performed in an ATR-FTIR cell with [EMI+][TFSI−] electrolyte, in which a ZnSe hemicylinder prism was covered with SLG as the working electrode, with platinum wires as the counter and reference electrodes (Fig. 3a). The imaginary (C_{im}) and real (C_{re}) parts of the capacitance vs. frequency curves at 0 V are shown in Fig. 3b, where C_{im} and C_{re} were obtained using the method developed by Taberna et al.[43] (Eq. (8) and Eq. (9) in the Supporting information). As expected, C_{re}, which is related to the EDL capacitance, increases as the frequency decreases, while C_{im}, corresponding to the energy dissipation[43], shows a maximum at frequency f_0, known as 'knee frequency'[43,44]. The interfacial capacitance can be calculated as $C_{interface} = 2C_{re}$ (f_0) [31,43], which consists of the Helmholtz capacitance (C_H) and quantum capacitance (C_Q) in series, *i.e.*, $1/C_{interface}=1/C_H+1/C_Q$[13]. Fig. 3c shows an asymmetric V-shaped $C_{interface}$-voltage curve with respect to the potential of zero charge (PZC) at ~ −0.2 V, which is explained by the minimum quantum capacitance near the Dirac point[12,13]. Fig. 3d shows that f_0 shifts to a lower value (*e.g.*, from ~25 to ~10 Hz) for more positive polarization while keeping a constant value (~17.8 Hz) for negative polarization. Such a difference suggests that the time response of ions (with a time constant $\tau_0 = 1/2\pi f_0$) in the EDL is more susceptible to positive potential, which could be caused by the different ionic kinetics and charging mechanisms for positive or negative polarization. The constant f_0 under negative polarization is consistent with the unchanged mass of ions on SLG as obtained from the EQCM study[31], which is related to the immobile ion flux in such a situation. Under positive polarization, in contrast, the cluster-like escape of ions from SLG causes a marked change in knee frequency. The Nyquist plots in Fig. 3e show the shift of low-frequency capacitance toward smaller resistive values as the potential deviates from PZC, implying that the migration barriers of [EMI+] and [TFSI−] are dependent on the applied potential[43]. After 5 cycles of CV testing, EIS shows that the value of PZC shifts to −0.3 V, and the knee frequency is reduced under positive polarization (Figs. S4 and S7). The negative shift of PZC may be explained by the gradual change in SLG caused by the stronger interaction between adsorbed cations and SLG. However, the PZC remains nearly constant over more cycles, indicating that the [EMI+] absorption on SLG at PZC is quite stable, as shown in Fig. S8.

In situ ATR-FTIR spectroscopy is sensitive to s- or p- po-

CSTR: 32290.14.JUSTC-2024-0135
DOI: 32290.14.JUSTC-2024-0135
JUSTC, **2026**, 55(X):

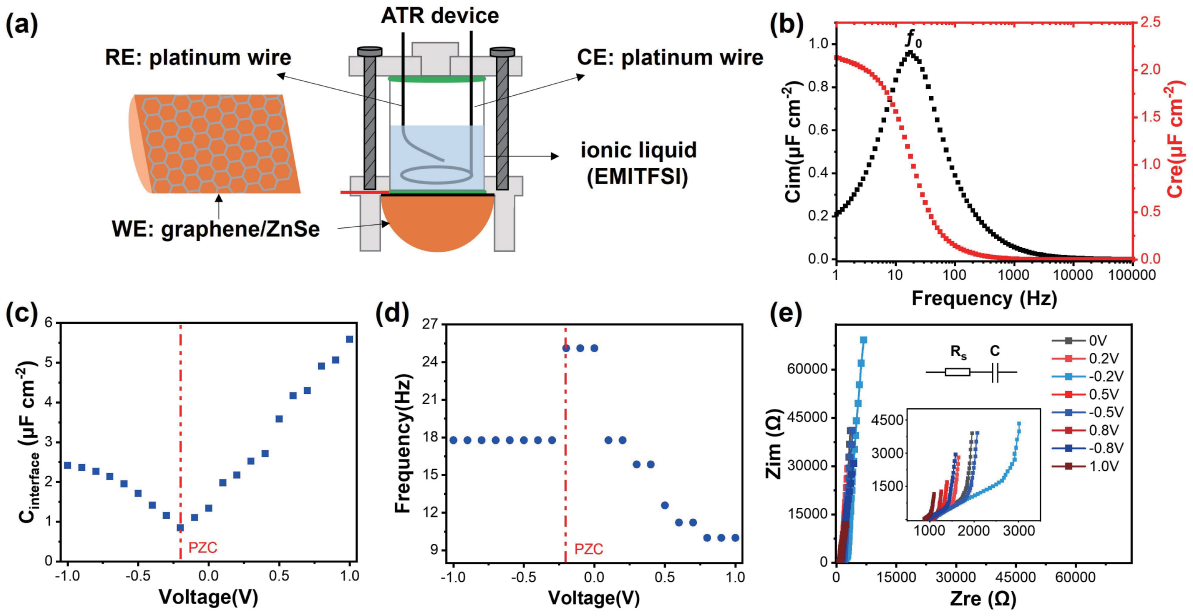

Fig. 3. (a) Schematic of the ATR-FTIR device for electrochemical testing. (b) Imaginary part (C_{im}, black dots) and real part (C_{re}, red dots) of the capacitance for the SLG-on-ZnSe electrode in [EMI$^+$][TFSI$^-$] at 0 V. (c) $C_{interface}$-voltage and (d) knee frequency (f_0)-voltage curves of SLG in [EMI$^+$][TFSI$^-$]. (e) Nyquist plots of SLG in [EMI$^+$][TFSI$^-$] obtained at different potentials before CV testing; the inset magnifies the high-frequency region and shows the equivalent circuit model.

larized light absorption of ions on SLG. The absorption of s-polarized light (A_s) is only related to the y component (A_y) of a transition dipole moment, while the x component (A_x) and z component (A_z) are attributed to the absorption of p-polarized light (A_p)[45], based on the definition of coordinates in Fig. 4a. Combining Eqs. 12 to 16 in the Supporting Information, A_s and A_p can be described as[46]

$$A_s = A_y \approx 1.54 \times NM^2 \sin^2\alpha \quad (1)$$

$$\text{and } A_p = A_x + A_z \approx NM^2 \times \left[0.71 + \left(\frac{19.44}{n_2^4} - 0.71\right)\cos^2\alpha\right], \quad (2)$$

where n_2 is the refractive index of graphene, N is the population of the transition dipole moment M, and α is the average tilting angle between the vector normal to the SLG surface and the dipole moment vector, as shown in Fig. 4b. A more detailed mathematical derivation can be found in the supplementary information. Based on Equations (1) and (2), we can see that A_s monotonously depends on N or α, while A_p increases when n_2 or α decreases or N increases. As shown in Fig. S9, n_2 remains nearly constant within the range of 0.01 e^-/h^+ charge injection, which could be estimated from CV measurements[25]. Fig. S10 shows the IR spectra of [EMI$^+$][TFSI$^-$] on the SLG surface under different potentials. The characteristic absorbance at ~1575 cm^{-1} for [EMI$^+$] and that at ~1051 cm^{-1} for [TFSI$^-$] are selected for further analysis, corresponding to the in-plane symmetric/antisymmetric stretching vibration of imidazole rings in [EMI$^+$] (ν(EMI$^+$)$_{ring}$) and the antisymmetric stretching vibration of the S-N-S bond in [TFSI$^-$] (ν_{as}(S-N-S))[47]. The absorbance of the ν(EMI$^+$)$_{ring}$ and ν_{as}(S-N-S) in response to the applied potential is shown in Fig. 4c and d, respectively. The insets in Fig. 4c and d show the vibration models for ν(EMI$^+$)$_{ring}$ and ν_{as}(S-N-S), which are also shown in Movies S1 to S3). From Fig. 4c and d, we can see that the absorbance of A_s shows the maximum, but A_p shows the minimum for both [EMI$^+$] and [TFSI$^-$] for the applied potential at PZC (~ −0.3 V). When the electrode is negatively charged, A_s decreases and A_p increases for both [EMI$^+$] and [TFSI$^-$]. For a positive potential below ~ +0.6 V, A_s and A_p of [EMI$^+$] and [TFSI$^-$] show a trend similar to the situation of negative polarization, but when the positive potential is higher than ~ +0.6 V, the A_p of [EMI$^+$] decreases.

Now, we combine in situ ATR-FTIR results, DFT simulations and the mathematical relationship between A_s, A_p and N, M, α, and n_2, as shown in Equations (1) and (2), to analyze the ionic behavior on SLG, as schematically illustrated in Fig. 4e and f. Based on DFT simulations, the frequency of the ν(EMI$^+$)ring or ν_{as}(S-N-S) is not sensitive to the cluster size of [EMI$^+$][TFSI$^-$], as verified by the simulations in Fig. S11. The electron dipole moment M of the vibrations was calculated by DFT (method in Supporting Information), as shown in Fig. S12. Our results show that the orientation of M for ν(EMI$^+$)$_{ring}$ is nearly parallel to the imidazole ring, while the orientation of M for ν_{as}(S-N-S) is perpendicular to the angular bisector of [TFSI$^-$], as labeled in the insets of Fig. 4e and f. Due to van der Waals interactions[48], the imidazole ring of [EMI$^+$] is mostly parallel to the SLG surface at PZC. However, it is difficult to determine the spatial alignment of [TFSI$^-$] at PZC since [TFSI$^-$] could rotate around the dipole moment vector M for ν_{as}(S-N-S). Under negative polarization, the N value for [EMI$^+$] is presumed to increase due to counterion adsorption[42]; thus, the α value will decrease to yield the observed decrease in A_s shown in Fig. 4c, corresponding to the tilting of the imidazole ring of [EMI$^+$] in the EDL, as schematically shown in Fig. 4e. For [EMI$^+$] under positive polarization below ~ +0.6 V, the A_p value increases with the voltage, indicating an increase in $\cos^2(\alpha)$ and a decrease in α, corres-

CSTR: 32290.14.JUSTC-2024-0135
DOI: 32290.14.JUSTC-2024-0135
JUSTC, **2026**, 55(X):

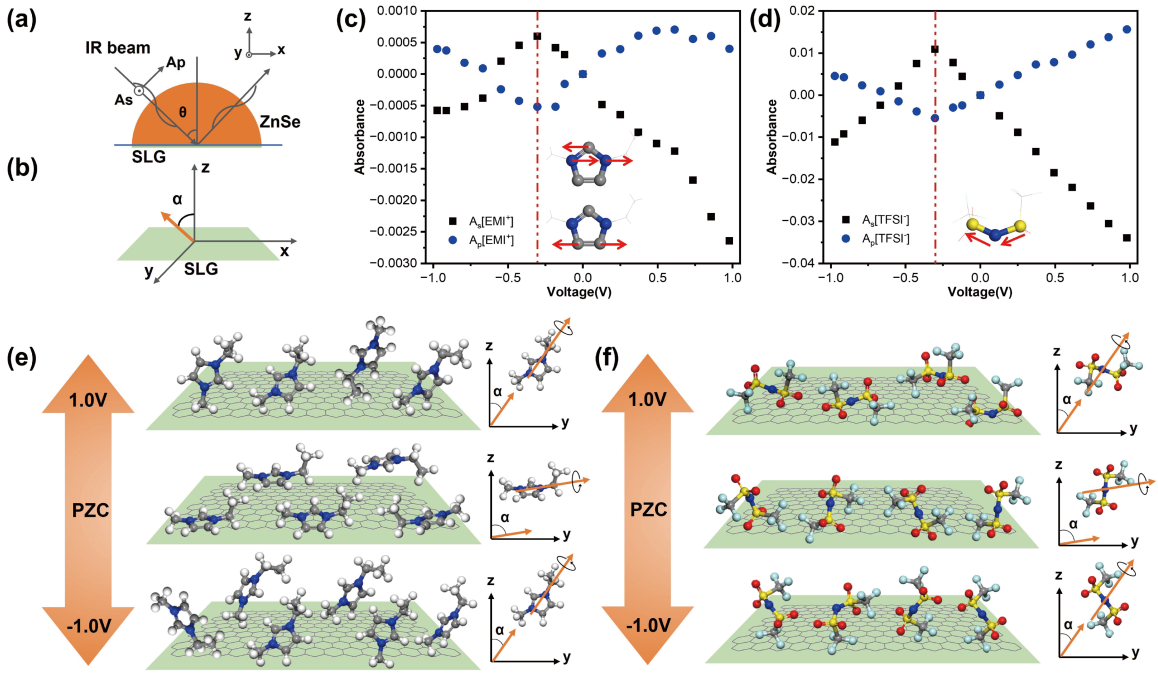

Fig. 4. Illustration of the coordination of (a) A_s, A_p and (b) tilting angle α. In situ ATR-FTIR absorbance of (c) [EMI+] and (d) [TFSI−] with S-polarization and P-polarization under different potentials. The reference spectrum was collected at ~0 V. Proposed molecular configurations of (e) cations and (f) anions at the SLG/[EMI+][TFSI−] interface under different potentials. The orange arrows in the right inset show the orientation axis of the transition dipole moment, around which the ions can rotate. The carbon, nitrogen, hydrogen, sulfur, oxygen and fluorine atoms are denoted as gray, blue, white, yellow, red and cyan balls, respectively.

ponding to a tilted [EMI+] rearrangement, as the N value of [EMI+] is supposed to decrease at such a polarization voltage. Under a positive polarization higher than ~ +0.6 V, the N for [EMI+] decreases more significantly, leading to a decrease in A_s and A_p, as shown in Fig. 4c, showing that the desorption of [EMI+] dominates the A_s and A_p signals. We should note that since the effective depth of penetration for p-polarized light is larger than that of s-polarized light[42], the bipolar A_p peak of $\nu(EMI^+)_{ring}$ (Fig. S10d) might consist of contributions from [EMI+] in the solution and [EMI+] absorbed on SLG. On the other hand, the N value for [TFSI−] should decrease under negative polarization, but it is hard to determine the changing trend of α solely based on Equation (1). Based on Equation (2), when the A_p value increases at voltages deviating from PZC, as observed in Fig. 4d, the $\cos^2(\alpha)$ value has to remarkably increase to eliminate the influence of a decrease in N. That is, α decreases for negative polarization. Under positive polarization, the N for [TFSI−] increases, necessitating a reduced α to yield the observed decrease in A_s, as shown in Fig. 4f. Extra in situ ATR FTIR spectroscopy was performed within −1.0 V~ 1.0 V (Fig. S13), from which the potential corresponding to the minimum absorbance, *i.e.*, the value of PZC, decreases from ~ −0.3 V to ~ −0.4 V after 5 cycles, similar to the result of EIS as presented above.

Although the estimated IR detection depth (0.9 to 1.7 μm, see Supporting Information) is much larger than the Debye length of the IL (typically 1-4 nm[49]), we think the difference in the signal is mainly attributed to the change in several ionic layers on SLG, as the molecular dynamics study has shown that the distribution of ions on SLG transits to the bulk in approximately 3-4 nm (Fig. S14). Now, we discuss the ionic configuration based on the IR data shown above. First, we can deduce that the tilting angle α shows a maximum at a PZC of ~ −0.3 V, *i.e.*, a 'flatter' state for the orientation axis of the transition dipole moment. Under potentials, although the molecule may rotate along the vector α while keeping the direction of the dipole moment unchanged, we can still obtain some hints on the relationship between the ionic configuration and the electrochemical behavior at the SLG/[EMI+][TFSI−] interface. For the adsorption [EMI+], the decrease in tilting angle α means a more vertical arrangement of the imidazole ring, which, in principle, leads to an increased adsorption of [EMI+] per area. The vertical standing of [EMI+], however, would increase the distance (defined as the $d_{charge\ surface}$) between the positive charge center (in the plane of the imidazole ring) and the SLG. These two factors compete in a thermal dynamic process. Controlled by the total energy profit of cations and anions, the decreased α for [EMI+] may be accompanied by the reorganization of [EMI+]/[TFSI−] packing yet with increased [EMI+] adsorption density, especially at negative potentials, explaining the previous observation of unchanged adsorption mass measured by EQCM[31] and similar findings by MD simulations[31,50]. Such a configuration of [EMI+] can also explain the mild change in capacitance, as observed in Fig. 3c, and little change in frequency, as shown in Fig. 3d, for potentials lower than ~ −0.2 V. For [TFSI−], the decrease in α at positive potentials may result in a variety of possible alignments on SLG, resulting in an increased adsorption density. Considering a previous study reporting that the $d_{charge\ surface}$ of [TFSI−] is decreased under positive potentials[25], positive polarization would cause a more significant impact on charge storage. Especially accom-

CSTR: 32290.14.JUSTC-2024-0135
DOI: 32290.14.JUSTC-2024-0135
JUSTC, **2026**, 55(X):

panied by the cluster-like desorption of $[EMI_{1.58},TFSI_{0.58}]^+$ [31], a more dense rearrangement of [$TFSI^-$] on SLG is in agreement with the experimental observation of a more obviously increased capacitance and lowered knee frequency under positive polarization, as shown in Fig. 3c.

4 Conclusions

The ionic behavior of [EMI^+][$TFSI^-$] on SLG has been investigated on a molecular level and in real time with in situ ATR-FTIR spectroscopy in combination with ex situ Raman spectroscopy, electrochemical characterization and DFT simulations. We have observed that SLG has irreversible electrochemical doping during charge/discharge within −1~1 V and an irreversible structural change in the voltage range of >1.75 V or < −2.0 V. Our in situ ATR-FTIR revealed a decreased titling angle α of [EMI^+], which could be related to a more closely packed vertical arrangement in the reorganization between [EMI^+] and [$TFSI^-$] under negative polarization. Under positive polarization, the rearrangement of [$TFSI^-$] results in more significant changes in adsorption density and capacitance. We expect that the fundamental understanding of ion behavior can provide deeper insight into the EDL structure at the ionic liquid/SLG interface, thus serving as guidance for the design of better carbon-based supercapacitors. The potential impact of this work may include (a) tailoring the structure of the carbon electrode to coordinate the competition between the adsorption density of ions and the distance between the charge center and carbon surface, thus maximizing the interfacial ion arrangement density, and (b) incorporating additives to adjust the charge center of cations or anions in ionic liquids to modulate the EDL structure.

Supporting information

The supporting information for this article can be found online at https://doi.org/10.52396/JUSTC-2024-0135. The supporting information includes the analytical methods of EIS and ATR-FTIR and 14 figures.

Acknowledgements

This work was supported by the National Key R&D Program of China (Grant No. 2020YFA0711502), National Natural Science Foundation of China (Grant Nos. 52273234, 52325202, 22172151), and Fundamental Research Funds for the Central Universities (WK2060000098). The USTC Center for Micro and Nanoscale Research and Fabrication, the Supercomputing Center of USTC and the Hefei Advanced Computing Center are appreciated.

Conflict of interest

The authors declare that they have no conflict of interest.

References

[1] El-Kady M F, Shao Y, Kaner R B. Graphene for batteries, supercapacitors and beyond. *Nature Reviews Materials*, **2016**, *1*: 16033

[2] Kang M S, Heo I, Cho K G, et al. Coarsening-induced hierarchically interconnected porous carbon polyhedrons for stretchable ionogel-based supercapacitors. *Energy Storage Materials*, **2022**, *45*: 380–388

[3] Li Y B, Zhang D Y, Zhang Y M, et al. Biomass-derived microporous carbon with large micropore size for high-performance supercapacitors. *Journal of Power Sources*, **2020**, *448*: 227396

[4] Zhang H Z, Tian J Y, Cui X K, et al. Highly mesoporous carbon nanofiber electrodes with ultrahigh specific surface area for efficient capacitive deionization. *Carbon*, **2023**, *201*: 920–929

[5] Zhu Y W, Murali S, Stoller M D, et al. Carbon-based supercapacitors produced by activation of graphene. *Science*, **2011**, *332* (6037): 1537–1541

[6] Simon P, Gogotsi Y. Perspectives for electrochemical capacitors and related devices. *Nature materials*, **2020**, *19*: 1151–1163

[7] Raccichini R, Varzi A, Passerini S, et al. The role of graphene for electrochemical energy storage. *Nature Materials*, **2015**, *14*: 271–279

[8] Liu D B, Ni K, Ye J L, et al. Tailoring the structure of carbon nanomaterials toward high-end energy applications. *Advanced Materials*, **2018**, *30* (48): 1802104

[9] Li Z N, Gadipelli S, Li H C, et al. Tuning the interlayer spacing of graphene laminate films for efficient pore utilization towards compact capacitive energy storage. *Nature Energy*, **2020**, *5*: 160–168

[10] Tan J, Li Z H, Ye M X, et al. Nanoconfined space: Revisiting the charge storage mechanism of electric double layer capacitors. *ACS Applied Materials & Interfaces*, **2022**, *14* (33): 37259–37269

[11] Conway B E. Electrochemical Supercapacitors: Scientific Fundamentals and Technological Applications. New York: *Springer New York*, **2013**

[12] Xia J, Chen F, Li J, et al. Measurement of the quantum capacitance of graphene. *Nature Nanotechnology*, **2009**, *4*: 505–509

[13] Ji H X, Zhao X, Qiao Z H, et al. Capacitance of carbon-based electrical double-layer capacitors. *Nature Communications*, **2014**, *5*: 3317

[14] Forse A C, Merlet C, Griffin J M, et al. New perspectives on the charging mechanisms of supercapacitors. *Journal of the American Chemical Society*, **2016**, *138* (18): 5731–5744

[15] Largeot C, Portet C, Chmiola J, et al. Relation between the ion size and pore size for an electric double-layer capacitor. *Journal of the American Chemical Society*, **2008**, *130* (9): 2730–2731

[16] Chmiola J, Yushin G, Gogotsi Y, et al. Anomalous increase in carbon capacitance at pore sizes less than 1 nanometer. *Science*, **2006**, *313* (5794): 1760–1763

[17] Griffin J M, Forse A C, Tsai W Y, et al. *In situ* NMR and electrochemical quartz crystal microbalance techniques reveal the structure of the electrical double layer in supercapacitors. *Nature Materials*, **2015**, *14* (8): 812–819

[18] Tsai W Y, Taberna P L, Simon P. Electrochemical quartz crystal microbalance (EQCM) study of ion dynamics in nanoporous carbons. *Journal of the American Chemical Society*, **2014**, *136* (24): 8722–8728

[19] Prehal C, Koczwara C, Jäckel N, et al. Quantification of ion confinement and desolvation in nanoporous carbon supercapacitors with modelling and *in situ* X-ray scattering. *Nature Energy*, **2017**, *2*: 16215

[20] Chmiola J, Largeot C, Taberna P L, et al. Desolvation of ions in subnanometer pores and its effect on capacitance and double-layer theory. *Angewandte Chemie International Edition*, **2008**, *47* (18): 3392–3395

[21] Futamura R, Iiyama T, Takasaki Y, et al. Partial breaking of the Coulombic ordering of ionic liquids confined in carbon nanopores. *Nature Materials*, **2017**, *16*: 1225–1232

[22] Wu P, Huang J, Meunier V, et al. Complex capacitance scaling in ionic liquids-filled nanopores. *ACS Nano*, **2011**, *5* (11): 9044–9051

[23] Uysal A, Zhou H, Feng G, et al. Structural origins of potential dependent hysteresis at the electrified graphene/ionic liquid

CSTR: 32290.14.JUSTC-2024-0135
DOI: 32290.14.JUSTC-2024-0135
JUSTC, **2026**, 55(X):

interface. *The Journal of Physical Chemistry C*, **2014**, *118* (1): 569–574

[24] Xu K, Lin Z, Merlet C, et al. Tracking ionic rearrangements and interpreting dynamic volumetric changes in two-dimensional metal carbide supercapacitors: A molecular dynamics simulation study. *ChemSusChem*, **2018**, *11* (12): 1892–1899

[25] Zhou S, Panse K S, Motevaselian M H, et al. Three-dimensional molecular mapping of ionic liquids at electrified interfaces. *ACS Nano*, **2020**, *14* (12): 17515–17523

[26] Fleischmann S, Zhang Y, Wang X, et al. Continuous transition from double-layer to Faradaic charge storage in confined electrolytes. *Nature Energy*, **2022**, *7*: 222–228

[27] Paek E, Pak A J, Hwang G S. A computational study of the interfacial structure and capacitance of graphene in [BMIM][PF_6] ionic liquid. *Journal of The Electrochemical Society,* **2012**, 160 (1): A1

[28] Xu S, Xing S, Pei S S, et al. Sum frequency generation spectroscopy study of an ionic liquid at a graphene-BaF_2 (111) interface. *The Journal of Physical Chemistry B*, **2014**, *118* (19): 5203–5210

[29] Uysal A, Zhou H, Feng G, et al. Structural origins of potential dependent hysteresis at the electrified graphene/ionic liquid interface. *The Journal of Physical Chemistry C*, **2014**, *118* (1): 569–574

[30] Xu S, Xing S, Pei S S, et al. Molecular response of 1-butyl-3-methylimidazolium dicyanamide ionic liquid at the graphene electrode interface investigated by sum frequency generation spectroscopy and molecular dynamics simulations. *The Journal of Physical Chemistry C*, **2015**, *119* (46): 26009–26019

[31] Ye J, Wu Y C, Xu K, et al. Charge storage mechanisms of single-layer graphene in ionic liquid. *Journal of the American Chemical Society*, **2019**, *141* (42): 16559–16563

[32] Wu Y C, Ye J, Jiang G, et al. Electrochemical characterization of single layer graphene/electrolyte interface: Effect of solvent on the interfacial capacitance. *Angewandte Chemie International Edition*, **2021**, *60* (24): 13317–13322

[33] Ferrari A C, Meyer J C, Scardaci V, et al. Raman spectrum of graphene and graphene layers. *Physical Review Letters*, **2006**, *97* (18): 187401

[34] Yasuda S, Kumagai R, Nakashima K, et al. Electrochemical potential stabilization of reconstructed Au(111) structure by monolayer coverage with graphene. *The Journal of Physical Chemistry Letters*, **2015**, *6* (17): 3403–3409

[35] Froehlicher G, Berciaud S. Raman spectroscopy of electrochemically gated graphene transistors: Geometrical capacitance, electron-phonon, electron-electron, and electron-defect scattering. *Physical Review B*, **2015**, *91* (20): 205413

[36] Zhong J H, Liu J Y, Li Q, et al. Interfacial capacitance of graphene: Correlated differential capacitance and in situ electrochemical Raman spectroscopy study. *Electrochimica Acta*, **2013**, *110*: 754–761

[37] Das A, Pisana S, Chakraborty B, et al. Monitoring dopants by Raman scattering in an electrochemically top-gated graphene transistor. *Nature Nanotechnology*, **2008**, *3*: 210–215

[38] Basko D M, Piscanec S, Ferrari A C. Electron-electron interactions and doping dependence of the two-phonon Raman intensity in graphene. *Physical Review B*, **2009**, *80* (16): 165413

[39] Hu G, Pandey G P, Liu Q, et al. Self-organization of ions at the interface between graphene and ionic liquid DEME-TFSI. *ACS Applied Materials & Interfaces*, **2017**, *9* (40): 35437–35443

[40] Zhang Y, Hu G, Gong M, et al. Lateral graphene p–n junctions realized by nanoscale bipolar doping using surface electric dipoles and self‐organized molecular anions. *Advanced Materials Interfaces*, **2019**, *6* (1): 1801380

[41] Li J, Tang J, Yuan J, et al. Interactions between graphene and ionic liquid electrolyte in supercapacitors. *Electrochimica Acta*, **2016**, *197*: 84–91

[42] Romann T, Oll O, Pikma P, et al. Surface chemistry of carbon electrodes in 1-ethyl-3-methylimidazolium tetrafluoroborate ionic liquid-an in situ infrared study. *Electrochimica Acta*, **2014**, *125*: 183–190

[43] Taberna P L, Simon P, Fauvarque J F. Electrochemical characteristics and impedance spectroscopy studies of carbon-carbon supercapacitors. *Journal of the Electrochemical Society*, **2003**, *150* (3): A292

[44] Hughes M, Shaffer M S P, Renouf A C, et al. Electrochemical capacitance of nanocomposite films formed by coating aligned arrays of carbon nanotubes with polypyrrole. *Advanced Materials*, **2002**, *14* (5): 382–385

[45] Vallant T, Kattner J, Brunner H, et al. Investigation of the formation and structure of self-assembled alkylsiloxane monolayers on silicon using in situ attenuated total reflection infrared spectroscopy. *Langmuir*, **1999**, *15* (16): 5339–5346

[46] Ras R H A, Schoonheydt R A, Johnston C T. Relation between s-polarized and p-polarized internal reflection spectra: application for the spectral resolution of perpendicular vibrational modes. *The Journal of Physical Chemistry A*, **2007**, *111* (36): 8787–8791

[47] Kiefer J, Fries J, Leipertz A. Experimental vibrational study of imidazolium-based ionic liquids: Raman and infrared spectra of 1-ethyl-3-methylimidazolium bis (trifluoromethylsulfonyl) imide and 1-ethyl-3-methylimidazolium ethylsulfate. *Applied Spectroscopy*, **2007**, *61* (12): 1306–1311

[48] Zhou H, Rouha M, Feng G, et al. Nanoscale perturbations of room temperature ionic liquid structure at charged and uncharged interfaces. *ACS Nano*, **2012**, *6* (11): 9818–9827

[49] Min Y, Akbulut M, Sangoro J R, et al. Measurement of forces across room temperature ionic liquids between mica surfaces. *The Journal of Physical Chemistry C*, **2009**, *113* (37): 16445–16449

[50] Begić S, Jónsson E, Chen F, et al. Molecular dynamics simulations of pyrrolidinium and imidazolium ionic liquids at graphene interfaces. *Physical Chemistry Chemical Physics*, **2017**, *19* (44): 30010–30020

CSTR: 32290.14.JUSTC-2024-0135
DOI: 32290.14.JUSTC-2024-0135
JUSTC, **2026**, 55(X):